# OMAE2020-18935

# RELATIVE MOTION DURING SINGLE BLADE INSTALLATION: MEASUREMENTS FROM THE NORTH SEA

**Aljoscha Sander**[*]
University of Bremen
Bremen, Germany
Email: alsander@uni-bremen.de

**Andreas F. Haselsteiner**
University of Bremen
Bremen, Germany
Email: a.haselsteiner@uni-bremen.de

**Kader Barat**
University of Bremen
Bremen, Germany
Email: baratk@uni-bremen.de

**Michael Janssen**
University of Bremen
Bremen, Germany
Email: janszen@uni-bremen.de

**Stephan Oelker**
University of Bremen
Bremen, Germany
Email: soelker@uni-bremen.de

**Jan-Hendrik Ohlendorf**
University of Bremen
Bremen, Germany
Email: johlendorf@uni-bremen.de

**Klaus-Dieter Thoben**
University of Bremen
Bremen, Germany
Email: thoben@uni-bremen.de

## ABSTRACT

During single blade installation in offshore wind farms, relative motion between nacelle and blade root due to wind and wave excitation pose a significant challenge. Wave excitation can be modelled considerably well by employing state-of-the-art simulation tools and can, therefore, be included in installation planning. Other phenomena, such as flow-induced vibrations are hard to capture and hence challenging to account for when defining installation procedures and limitations. Here, we present measurements conducted during the installation of an offshore wind farm consisting of multi-megawatt turbines installed on monopile foundations in the North Sea. A custom-built sensor capturing linear & angular acceleration and GPS-data was deployed atop the nacelle. Both partially and fully assembled turbines displayed complex oscillation orbits, swiftly changing amplitude and direction. Mean nacelle deflection correlated strongly with significant wave height as well as mean wind speed. As wind speed and significant wave height showed a strong correlation as well, it is difficult to discern which load drives the observed relative motions. While wind loads are significantly smaller than wave loads on partially assembled turbines under installation conditions, additional momentum induced by vortex shedding may prove sufficient to cause the observed effects.

---

[*]Address all correspondence to this author.

## INTRODUCTION

The increasing demand for electricity coinciding with the transformation towards a carbon-neutral energy supply as well as the mature state of wind energy conversion technology has spurred an increase in offshore wind turbine (OWT) installation and subsequently resulted in ever growing OWTs. Larger wind turbines convert more energy per unit rotation as well as per installed turbine and thus are the main drivers to reduce the levelised cost of electricity (LCoE).

However, increasing turbines in size and mass as well as placing them offshore comes at a cost: Most OWTs are installed by jack up vessels or barges, commonly referred to as installation jack-up units (IJUs). Prior to installation the turbines or their components are loaded onto the IJU. Larger turbines require more vessel traffic between installation site and base port per installed offshore wind farm as with an increase in size, less turbines fit on one IJU. Additionally, the increase in size (mainly rotor diameter) complicates offshore installation. Except for rare concept cases, where the complete OWT is pre-assembled onshore and then transported as a whole to the installation site, OWTs are usually installed consecutively. Upon arrival at the installation site, the IJU jacks up, connects to the already installed transition piece (TP) and begins the installation by lifting the tower onto the TP. After tower installation, the nacelle, containing the drive train of the turbine is installed. Depending on the size of the OWT different options are possible for blade installation. For a rotor star installation, blades are pre-assembled with the rotor hub in the base port and, once the nacelle has been installed, the blade-hub assembly is lifted to nacelle height and installed. A derivative of the rotor-star installation is the bunny ear installation. Here, only two blades are pre-assembled with the hub and once the hub has been installed, the third blade follows. For larger turbines, these processes are no longer feasible. Instead, installations are carried out in a single blade installation process, where the hub is pre-installed on the nacelle and the blades are consecutively lifted and installed to the hub.

The combination of tower, nacelle and hub is sometimes referred to as a hammer configuration. Within the scope of this paper, the acronym TNH (tower-nacelle-hub-assembly) will be used to address the partially installed OWT.

While single blade installation allows for almost arbitrarily large blades, the installation process is sensitive to relative motion between rotor hub and the blade root. The large number of bolts that connect the blade to the hub require precise movements of the blade root during the mating process. Uncontrolled relative motions can severely disturb these operations, leading in turn to heavy delays and may thus increase installation costs significantly.

Relative motion between blade root and the rotor hub can have multiple causes:

- wave induced oscillations of the TNH
- wind induced oscillations of the TNH
- wind induced movements of the blade lifting device
- crane or human induced movements of the blade and the blade lifting device

Wave induced loads and thus deflections of the TNH make up the larger part of overall loads and thus are to be expected to cause most of the oscillations experienced by the TNH. In wave loads, the two most important parameters are the significant wave height $H_S$ and a parameter that describes wave periods, for example the wave peak period $T_P$. In soft-hard OWTs, the first eigenfrequency and $T_P$ are in close vicinity. Wave loads can be modelled fairly accurately by using potential theory, a variety of wave models and the Morison equation [1].

Wind induced loads are naturally much lower as densities of air and water differ roughly by a factor of 800. When designing OWTs, wind loads are usually split into two components: static loads and an additional dynamic component. However transient, aerodynamically induced vibrations are fairly complex and hard to account for as they are notoriously non-linear and dependent on a multitude of parameters, such as surface roughness, turbulence intensity, Reynolds number and mechanical properties of the structures involved. Vortex-induced vibrations are associated with a lock-in state, where the oscillation frequency and the vortex shedding frequency align, leading to large harmonic oscillating forces perpendicular to wind direction. This effect gained popularity as it caused the collapse of multiple large structures. Galloping and buffeting are both phenomena associated with additional transient forces with both lateral and streamwise components. While vortex-induced vibrations usually occur over longer periods of time (minutes to hours), buffeting and galloping can occur on smaller time scales. Standards and guidelines, such as EN-1991-1:2005 [2] account for these phenomena by two different engineering models, which can be used to account for vortex-induced vibrations when designing structures. However, these models are limited in their ability to predict these phenomena. It remains a key challenge to adequately capture these effects over a broad range of engineering applications.

While structures such as circular towers (in many cases simple cylinders even with a constant diameter) are prone to vortex-induced vibrations, blades and blade-lifting devices do not necessarily exhibit comparable phenomena during installation. However, due to complex geometries involved and the blade-lifting device being in essence a chaotic pendulum dangling from the crane, it is equally hard to correctly predict the behaviour during installation under wind loading. A few efforts have been undertaken to tackle this, e.g. [3–7].

Crane operations are conducted by humans and are thus subject to overcompensation and miscommunications between crane operator and installation crew. In installation planning this is usually accounted for by assuming a certain learning curve of personnel involved and thus an increased speed in installation time
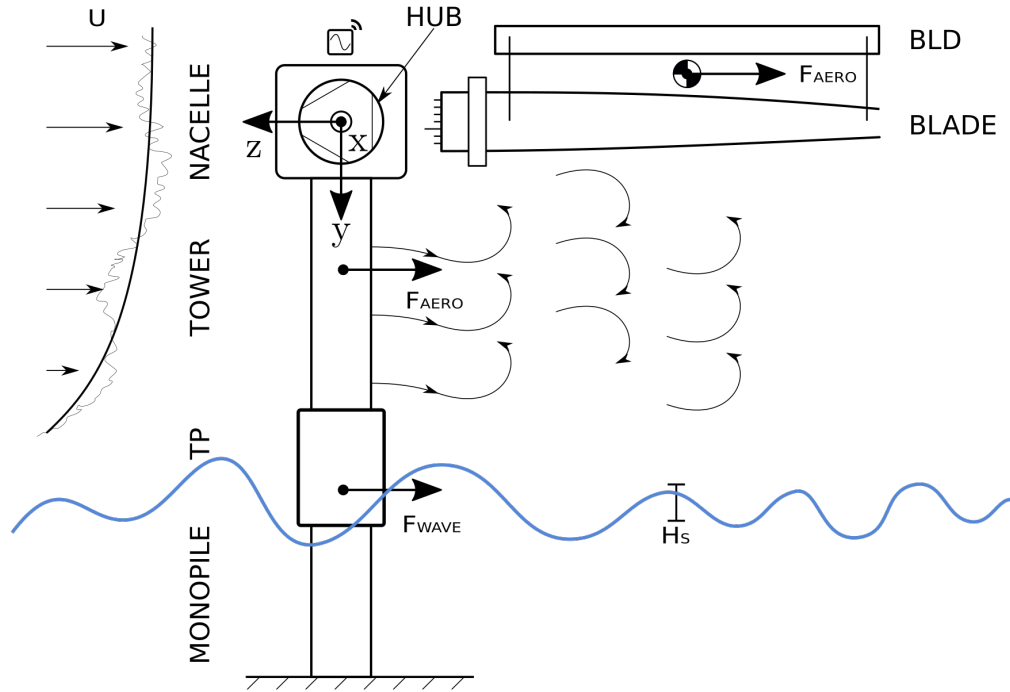
Figure 1: SET UP OF A TYPICAL OFFSHORE WIND TURBINE INSTALLATION AND THE DIFFERENT FORCES INVOLVED. BLD = BLADE LIFTING DEVICE. TP = TRANSITION PIECE.

per OWT.

A number of approaches have been developed to reduce oscillations occurring in OWTs both theoretically as well as tested in the field. Aerodynamic means include various forms of strakes and fairings. To mitigate oscillations mechanically, various forms of damping devices have been investigated [8–16].

Within this paper we present measurements of TNH oscillations, captured during installation operations of an offshore wind farm in the North Sea. Using a custom build measuring device, we recorded oscillations over a broad range of metocean conditions. We give a first description of oscillations encountered. This contribution is meant to be a starting point for tackling challenges arising from oscillations of offshore wind turbines during installation.

## DATA AND METHODS

The offshore wind turbines are multi-megawatt upwind turbines, installed in the North Sea. A total of 14 OWTs installations were monitored using the measuring device. The OWTs are of soft-hard type, resulting in eigenfrequency and wave peak period $T_P$ being in close vicinity. The hub height is approximately 35 $r_T$, monopile diameter is 2 $r_T$ and rotor radius is approxi-

mately 51 $r_T$, where $r_T$ is the tower radius [1]. The eigenfrequency of the TNH is approximately $f_E = 0.23\ Hz$ depending on water depth. The structural damping of the turbines is approximately 0.3%. Installation was carried out by utilizing a jack up vessel with a crane and storage capabilities for numerous offshore wind turbines. Foundations and transition pieces of the OWT were installed prior to OWT installation. Each installation includes in a consecutive manner the tower, the nacelle-hub assembly and each of the three blades. For each component specialized lifting devices are used. The blade lifting device has an overall length of 38 m, weighs approximately 60 t (without the blade) and includes hydraulics to securely grab the blade. For each blade, the blade lifting device is hooked to the crane of the IJU, directed to the blade rack to pick up a blade and finally lifted to hub height. Tuglines attached to the blade lifting device are used to carefully steer the blade root into the hub flange. A guiding pin is used to help the mating of blade root and flange. After a minimum number of bolts are secured, the blade lifting device is disengaged from the blade and returned to its grillage.

---

[1]To comply with OEM IP restrictions on turbine design, no units on the turbine's dimensions are given.

## Metocean Data

Environmental data was gathered by two different means: Aboard the IJU, a state-of-the-art Light detection and ranging device (LIDAR; WindCube, Leosphere, Orsay, France) system measured wind velocity at different heights, providing detailed wind field measurements. The measuring frequency of the LIDAR was 1 Hz. A wave buoy (Datawell Waverider, Datawell BV, Haarlem, The Netherlands), placed in the vicinity of the installation site (distance $< 5$ km, sampling frequency 5.12 Hz) recorded the sea state and provided sea state statistics for periods of 30 minutes. The wave buoy directly reported metocean parameters, such as wave peak period $T_P$, significant wave height $H_S$ and wave spreading $S$, the wave directional divergence angle at the peak frequency ($f_P = T_P^{-1}$). To enable data comparison, data was re-sampled to a period of 10 minutes. Wave data re-sampling (up-sampling as the wave buoy sample return periods were the longest) was done by employing a forward-fill method, replacing missing values from preceding sea states. For down-sampling an arithmetic mean of a sampling window of 10 minutes was used. All parameters denoted with a subscript of $_{10}$ - for example $H_{S10}$ or $T_{P10}$ - refer to the 10 minute mean of the corresponding parameter.

As the wave buoy only delivers discreetly modelled values for the wave peak period $T_P$, the wave zero up-crossing period $T_Z$ is used to calculate $T_P$. Under the assumption of a JONSWAP-spectrum and a peak enhancement factor of 3.3, $T_P$ can be calculated by:

$$T_P = 1.28 \cdot T_Z. \tag{1}$$

## Measurements

Measurements were conducted by installing a measuring device on the helicopter hoist platform of each nacelle during the offshore wind farm installation.

The measuring device was custom built to ensure the required sensitivity and to allow for different types of sensors; linear acceleration, linear angular momentum and magnetic field were captured by a 9-degrees-of-freedom inertial measurement unit (LSM9DF1, STMicroelectronics) at a sampling frequency of 30 Hz. Resolution of the linear acceleration sensor was set to $\pm 8$ g, where g corresponds to earth's gravitational acceleration. A GPS Sensor (GP-20U7) allowed for accurate temporal time-stamping as well as tracking of crane operations via GPS altitude and coordinates. Figure 2 shows the device installed on the nacelle as well as a close up with the device open.

A microcontroller (ESP32, running a custom firmware) fused the incoming data and using the GPS signal as well as the microprocessors internal real time clock, millisecond accuracy of measurements was achieved. Data was stored on a regular
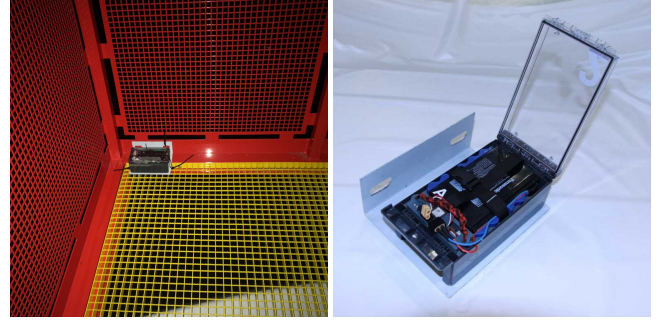


Figure 2: THE MEASURING DEVICE. LEFT HAND SIDE: ATOP THE NACELLE, STRAPPED TO THE HELICOPTER HOISTING PLATFORM. RIGHT HAND SIDE: DEVICE WITH LID OPEN, EXPOSING BATTERY AND ELECTRONICS.
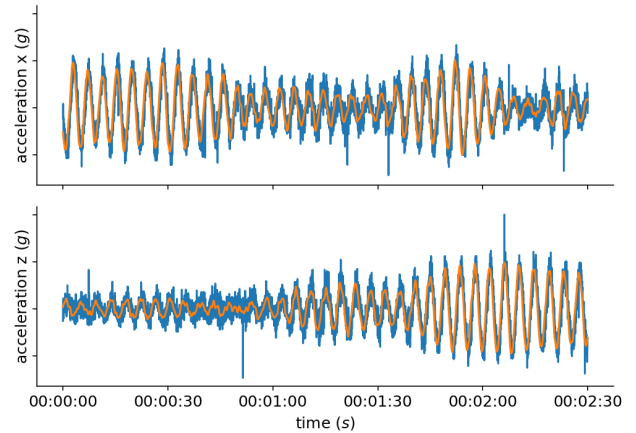


Figure 3: EXEMPLARY TIME SERIES RECORDED WITH THE MEASURING DEVICE FOR THE X (FORE-AFT) AND Z (SIDE-SIDE) COMPONENTS. BLUE LINES: RAW DATA. ORANGE LINES: RESAMPLED AND FILTERED DATA.

micro-SD card and between each installation, data was secured and stored on a server.

## Post-Processing, Integration and Data availability

In order to calculate the occurring deflections due to tower oscillations, accelerations were integrated twice. To ensure numerical stability, accelerations were first re-sampled to a constant time interval of 33 ms by employing forward-fill method, where preceding values are interpolated to a constant time stepping. This is necessary, as operations on the microcontroller of the measurement device caused minuscule time delays and thus could lead to non-constant time steps in the order of milliseconds in the data. We used a butterworth bandpass filter of 3rd
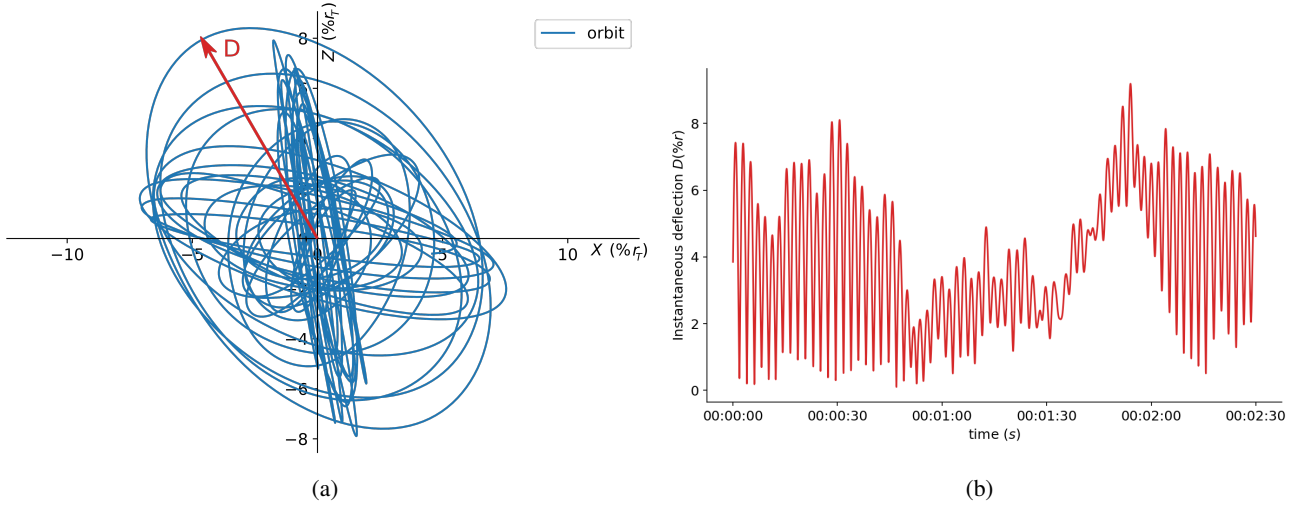
(a)                                    (b)

Figure 4: EXAMPLE OF AN OSCILLATION ORBIT IN THE FORE-AFT-LATERAL PLANE OF THE OWT (a). THE INSTAN-TANEOUS DEFLECTION $D$ IS SHOWN BY THE RED ARROW IN (a) AND CORRESPONDS TO THE MAGNITUDE OF THE INSTANTANEOUS POSITION VECTOR. PLOTTING DEFLECTION OVER TIME YIELDS FIGURE (b).

order with lower and upper cut off frequencies set to 0.1 Hz and 1 Hz respectively. The cut off frequencies were chosen as it is assumed, that occurring oscillations would coinciding with the TNH eigenfrequency of approximately 0.23 Hz. Filtered accelerations were then integrated twice by applying the second order trapezoidal rule. Filtering was necessary, as very low and very high frequency signal components lead to instabilities in the numerical integration. All numerical operations were implemented in python3 utilizing the numerical library numpy as well as the data science framework pandas.

Numerical integration yielded both velocity $\mathbf{V}(t)$ and position $\mathbf{X}(t)$ of the measuring device. Plotting the instantaneous position of the measuring device in the fore-aft and side-side plane results in an orbit of the tower oscillation. Figure 4a depicts an exemplary orbit. As an indicator for the intensity of TNH oscillation, the magnitude $D$ of the instantaneous position $\mathbf{X}(t)$ projected onto the oscillation plane was calculated (see Figure 4 for a graphical representation):

$$D(t) = \sqrt{x(t)^2 + z(t)^2} \qquad (2)$$

where $x(t)$ and $z(t)$ are the instantaneous positions in the fore-aft and side-side direction, respectively. The $y$-component of the positional vector was neglected as it is rather small and the reduction in hub height due to the component is negligible. $D(t)$ corresponds to the absolute distance the nacelle sways from it's original position independent of direction. Applying a temporal average over a time window of 10 minutes and applying normalisation by tower radius $r$ results in the parameter $d_{10}$, such that:

$$d_{10} = \frac{D_{10}}{r_T} \qquad (3)$$

where $D_{10}$ is the 10 minute mean of the instantaneous deflection $\mathbf{X}$ and $r$ is the mean tower radius of the OWT. As a means to reduce parameter dependency, linear regressions were calculated for $d_{10}$ as functions of significant wave height $H_S$ and wind speed ($U$) respectively:

$$d_{10} = a_1 + b_1 \cdot H_S \qquad (4)$$

$$d_{10} = a_2 + b_2 \cdot U \qquad (5)$$

where $a_1$, $b_1$, $a_2$ and $b_2$ are estimated using linear regression. Plotting this ratio over other parameters, such as wind velocity $U$ or peak period $T_P$ yields an estimate as to which parameters might have additional influence onto tower deflection and thus causing non-linear behaviour.

Approximately 53 days and 19 hours of data were recorded, amounting to $1.53 \times 10^8$ datapoints which result in $1.1 \times 10^6$ recorded oscillation cycles. To account for unknown effects due to the added mass, aerodynamic damping or excitation of the blades only data between the finished installation of the nacelle
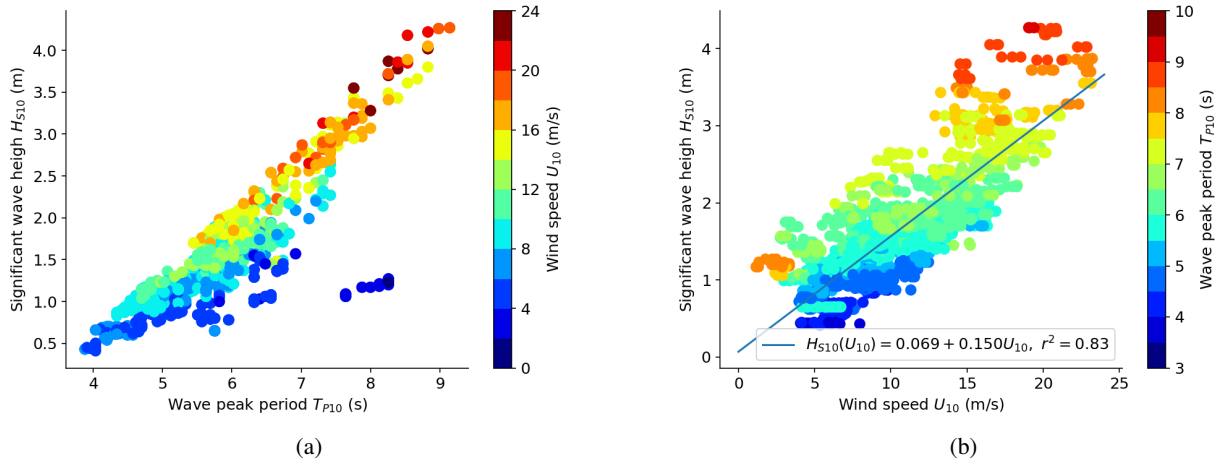
5

Figure 5: METOCEAN DATA FOR THE RECORDED DATA.

and the beginning of the first blade installation was selected from the raw data. This resulted in a total of 11 days and 10 hours ($8.1 \cdot 10^7$ data points and $5.91 \cdot 10^5$ oscillation cycles) of data.

## RESULTS

Figure 5a shows the sea states for the recorded installation times while Figure 5b depicts a scatter diagram for wind speed and wave height. Here a linear function is fitted using linear regression as well.

To gain insight into the behaviour of the turbines during installation, scatter diagrams are shown in Figure 6. A clear correlation between the 10 minute mean deflection ($d_{10}$, unit % tower radius $r_T$) and significant wave height ($H_{S10}$) can be observed (Figure 6a). Even for shallow waves ($H_{S10} < 0.75$ m) mean deflections reach values slightly below 4 % tower radius. Experience gained throughout the installation of the offshore wind farm showed, that blade installation becomes significantly harder to accomplish at sustained values of $d_{10} > 2.5$ %. For significant wave heights $H_{S10} > 2$ m, all measured mean deflections were larger than 2.5 %. The maximum observed deflection of 7.3 % occurred at a significant wave height of $H_{S10} = 1.9$ m, a peak period of $T_{P10} = 6$ s and a wind speed of $U_{10} = 14.4$ m/s. However, most observed values of $d_{10}$ remained below 6 % of tower radius, even for significant wave heights exceeding 4 m. Applying a linear regression, yields the following result:

$$d_{10}(H_S) = 1.436 + 1.088 \cdot H_S \tag{6}$$

The regression coefficient amounts to $r^2 = 0.72$.

Plotting mean deflection over wind velocity, a similar pattern emerges (Figure 6c). For wind speeds in excess of 15 m/s, all observed values for $d_{10}$ remain above 2.5 % tower radius, thus reducing the likelihood of successful blade installation significantly. At wind speeds of 6.8 m/s a sudden increase in mean deflection can be observed. For wind speed below 6.8 m/s, minimum deflections remain constant at approximately 0.5 % tower radius. Fitting a linear function to the data set reveals the following relation:

$$d_{10}(U) = 1.243 + 0.189 \cdot U \tag{7}$$

with a regression coefficient of $r^2 = 0.69$

Wave spreading, the deviation of the waves present in a sea state from their mean direction, has no real influence onto observed mean deflections. This is depicted in Figure 6e. Observed values for the wave spread span an interval from 10 deg to > 50 deg.

Combining mean deflection, wave peak period and significant wave height leads to Figure 6f. For peak periods below 4 s mean deflections are below 4 % for all observed data points. At 4 s peak period a sudden increase in mean deflection occurs, leading to mean deflections of $d_{10} > 5$ %. Color mapping the observed mean deflection to the significant wave height shows, that the waves coinciding with the sudden increase in mean deflections do not exceed significant wave heights of 2 m. Increasing wave peak period coincides with higher significant wave height while the non-linear spreading of mean deflection steadily decreases. For $H_{S10} > 3.5$ m, all mean deflections are above 4 %. Only a few data points exist for waves with a long peak period $T_P \approx 8$ s and significant wave heights $H_S \leq 2$ m. These waves are

assumed to be swell. The largest value for $d_{10} = 7.3$ % coincides with a peak period of $T_P = 6.3$ s. A similar mean deflection is observed at $T_P = 9$ s, coinciding with large waves ($H_S > 3.5$ m).

Assuming that the mean deflection is linearly dependent on the significant wave height and wind speed, combining Equation 4 and Equation 6 as well as Equation 5 and Equation 7 provides means to assess this assumption. If $d_{10}/d_{10}(H_S)$ or $d_{10}/d_{10}(H_S)$ respectively deviate from unity, a non-linear increase in mean deflection is observed. Values smaller than unity correspond to a non-linear decrease. The latter can be the case for low wind speeds at wave peak periods $> 5.5$ s (Figure 6b): here the ratio drops to values below 0.5. For wave peak periods $T_P < 6.5$ s and wind speed $U > 6.8$ m s$^{-1}$, a sudden increase of the ratio occurs - from $d_{10} \approx 0.25$ to $d_{10} > 0.5$ with the exception of a few outliers. With increasing wind speed, the deviations from unity of the ratio decrease. Even though long peak periods usually coincide with high values for significant wave height, deviations from the linear model are significantly reduced. For wind speeds between 5 m s$^{-1}$ and 10 m s$^{-1}$ increases in the ratio can exceed a value of 2 leading to more than the two-fold increase in mean deflection for a given significant wave height and wind speed. However, the spreading of the ratio in the given interval shows no clear correlation. Additionally, it has to be noted, that the highest increase in the ratio coincides with wave peak periods between 3.5 s $< T_P < 5$ s; with a period of $T_E = f_E^{-1} \approx 4.3$ s, where $f_E$ is the eigenfrequency of the TNH. Within this interval a dynamic response of the OWT to the wave peak period is to be expected.

A comparable pattern emerges when swapping abscissa and color-mapping in Figure 6d. A clear peak - with reduced width when comparing to the previous figure - can be observed for 4 s $< T_P < 5$ s, which is again in alignement with the eigenperiod of the OWT. Significant wave heights within this peak are limited to $H_{S10} \approx 1$ m. Again, as in the previous figure, the ratio between observed mean deflection and predicted linear mean deflection can exceed 2. Additionally, with increasing significant wave height and peak periods the ratio seems to converge towards unity, however, spreading remains larger when compared to Figure 6b.

## DISCUSSION & CONCLUSIONS
### Data and Methods
The results presented in this paper are based upon a measurement device which has a number of shortcomings: sensors are sensitive to thermal changes in the environment, which can cause non-linear drift. However, no indicators for non-linear noise have been identified in the data. Applying a narrow band-pass filter to the accelerations might lead to the suppression of low-frequency, wind-induced structural responses. But, as the accelerations of these low-frequency wind loads are small, they are assumed to be masked by noise in the acceleration signals

and are therefore hard to capture with MEMS-based acceleration measurements. Future sensor devices could capture these low-frequency accelerations by utilizing differential GPS, which yields the respective spatial resolution. Additionally, it has to be noted, that the sensor device has not undergone any certification. Applying more advanced data fusion algorithms, such as a Kalmann-Filter, should allow for an increase in accuracy and more detailed data, such as heading, pitch and yaw of the device. Simultaneous measurements at different positions during OWT installations are needed in order to capture the behaviour of all components involved (e.g. crane, ship, nacelle, hub, transition piece and lifting devices). LIDAR data with a sample frequency of 1 Hz proved to be sufficient, as this represents approximately 4 measurements per oscillation cycle. Wave data on the other hand had to be up-sampled to match the time-averaging window of 10 minutes. As the waves have a significant impact on oscillations, more detailed wave measurements should be conducted in future studies. Additionally, while the LIDAR was installed aboard the IJU during installation, the wave buoy was situated farther away. In future experiments the wave buoy should be moved with the IJU from installation site to installation site.

### Physical Interpretation of Mean Deflection and the Implications for Single Blade Installation
Experience from offshore personnel involved in the installation suggests, that single blade installation at mean deflections $d_{10} > 2.5$ % becomes unfeasible. This is, however, a mere observation and not supported by any experimental evidence. Nevertheless, a installation limit of $d_{10} < 2.5$ % would correspond to a mean significant wave height of $H_{S10} \approx 1$ m and a mean wind speed of $U_{10} \approx 7.5$ m s$^{-1}$, which in turn corresponds to a harsh installation limit for single blade installation. As waiting times of the installation vessel cause additional costs, more work is needed to investigate installation limits during single blade installation. Assuming a linear relation between mean deflection and significant wave height may be an oversimplification. Nevertheless, for mean deflections caused by significant wave heights greater than 3 m this seems to be a good estimate. Fitting a linear function to the mean deflection and mean wind speed shows a comparable agreement. This is, of course, due to the fact that wave height and wind speed exhibit a strong linear relationship as well (see linear fit in Figure 5b). Swell waves can be observed in Figure 6f and Figure 5a as a cluster of data points at a value of $T_{P10} \approx 8$ s and 1 m $< H_{S10} < 1.5$ m. The strong correlation between wind speed and significant wave height make it extremely difficult to discern between wind and wave loads with the data presented here and further research is needed. These should include correlations between deflection direction, wind and wave directions as well as correlations between structural response spectra and the spectra of metocean data to yield further insight into the main environmental load causing the relative
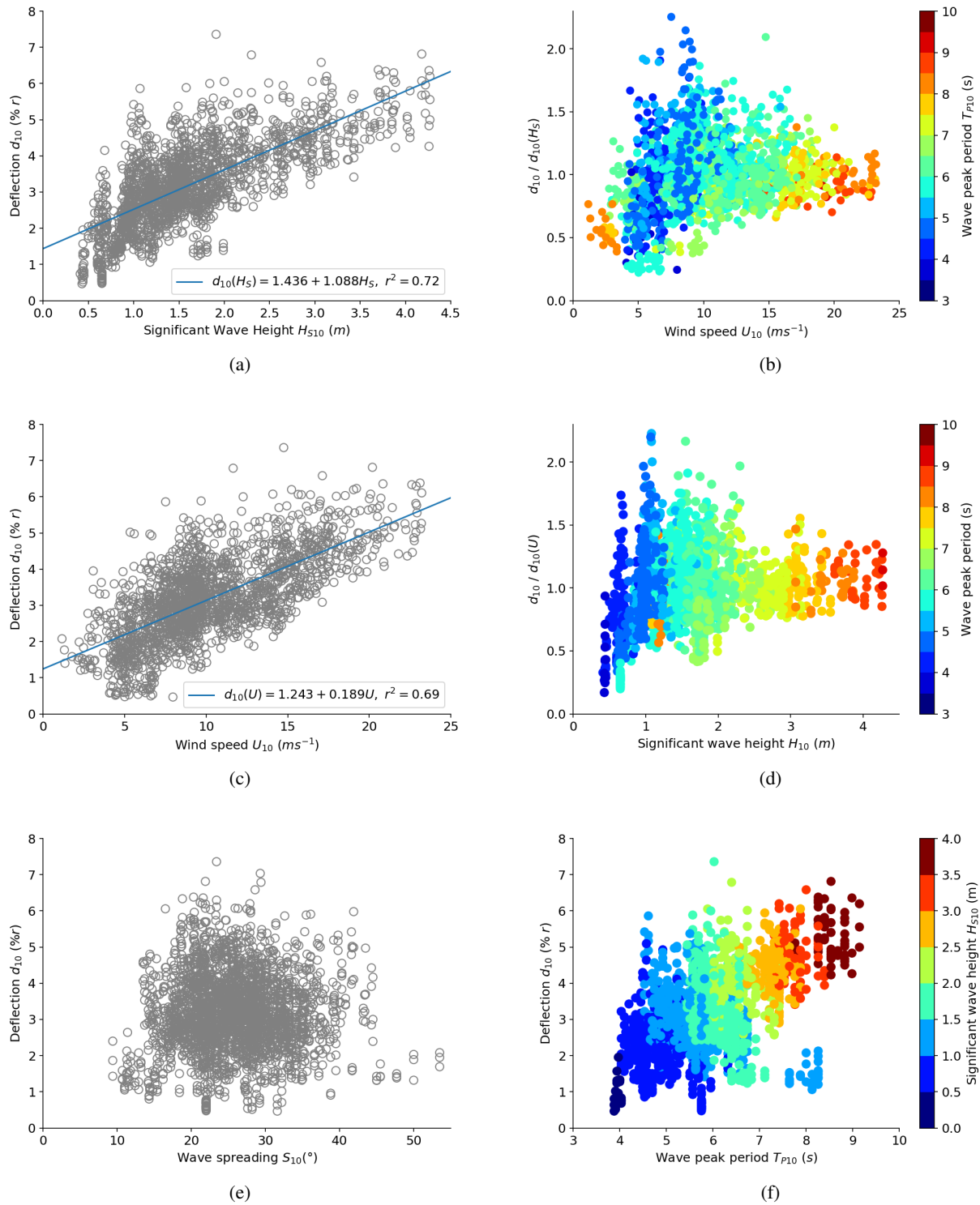
Figure 6: VISUALISATIONS OF THE MAIN PARAMETERS USED TO DESCRIBE THE PHENOMENON OF TNH OSCILLATIONS: WAVE PEAK PERIOD $T_{P10}$, SIGNIFICANT WAVE HEIGHT $H_{S10}$, WIND SPEED $U_{10}$, WAVE SPREADING $S_{10}$ AND MEAN DEFLECTION $d_{10}$.
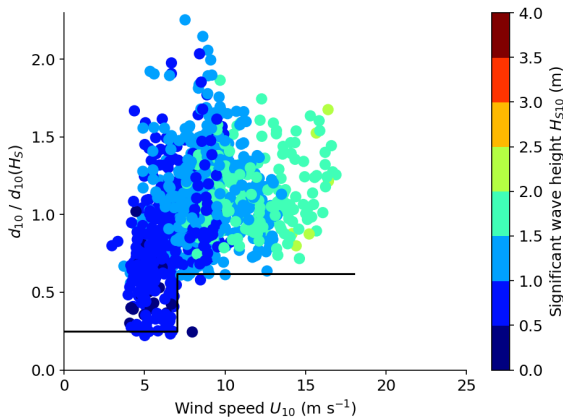
8

Figure 7: SCATTER DIAGRAM FOR MEAN DEFLECTION $d_{10}$ NORMALISED BY THE LINEAR FIT $d_{10}(H_S)$ OVER WIND SPEED (AS Figure 6b) BUT WITH WAVE PEAK PERIODS $T_{P10} > 6$ s REMOVED.

motions.

Dividing the mean deflection by linear functions fitted to match all observed mean deflections to wind speed or significant wave height eliminates the linear influence of the corresponding parameter, allowing for deviations from the linear model to emerge (Figure 6d and Figure 6b). Peak deviation from the linear models is most prominent for peak periods between 4 s and 5.5 s and wind speeds between 5 m s$^{-1}$ and 10 m s$^{-1}$. However, the presence of this combination does not necessarily lead to non-linear increases in mean deflection. In future analysis, all three parameters, $U$, $H_S$ and $T_p$ should be regarded, as the data presented here shows a certain response of TNH deflection to peak periods.

The abrupt - albeit small - increase of the deflection ratio $d_{10}/d_{10}(H_{S10})$ at wind speeds $U_{10} > 7$ m s$^{-1}$ could indicate aerodynamic effects, even though the effect is masked by a few outliers. To emphasize this, Figure 7 shows the mean deflection normalised with $d_{10}(H_S)$ but with peak periods of $T_{P10} > 6$ s removed as a few waves with long periods otherwise mask this jump.

Assuming a Strouhal number of St = 0.2 and by using the OWT tower diameter as a characteristic length and a wind speed of 7 m s$^{-1}$ as velocity, the estimated vortex shedding frequency aligns with OWT eigenfrequency. This could amplify aerodynamic effects on tower oscillation at these intermediate wind speeds. The sudden increase in mean deflection observed in Figure 6b for relatively low significant wave heights and values of 4 s $< T_{P10} < 5.5$ s could explain why even at favourable metocean conditions for single blade installation, installation attempts can fail.

In future analysis, measurements from the complete instal-

lation cycle should be accounted for to answer questions such as: how does the additional mass of the blades as well as the aerodynamic behaviour influence oscillations and consequently relative motion during installation? Additional excitation may occur if for example during the installation of the second blade, the already installed blade experiences vortex shedding at an adverse frequency. A special focus should be put onto what is causing the failure of the single blade installation: is it simply the mean deflection of the TNH at hub height itself, which cannot be matched by the blade lifting device and the crane and thus leads to failing attempts? And, consequently, if the phenomena are understood, what are feasible and safe ways to reduce oscillations and thus lead to the overall reduction in LCoE for offshore wind energy?

## ACKNOWLEDGMENT

## REFERENCES

[1] Morison, J. R., Johnson, J. W., and Schaaf, S. A., 1950. "The Force Exerted by Surface Waves on Piles". *Journal of Petroleum Technology,* **2**(05), May, pp. 149–154.

[2] DIN EN 1991-1-4:2010 Eurocode 1: Actions on structures.

[3] Jiang, Z., Gao, Z., Ren, Z., Li, Y., and Duan, L., 2018. "A parametric study on the final blade installation process for monopile wind turbines under rough environmental conditions". *Eng. Struct.,* **172**, Oct., pp. 1042–1056. WOS:000445440300076.

[4] Gaunaa, M., Bergami, L., Guntur, S., and Zahle, F., 2014. "First-order aerodynamic and aeroelastic behavior of a single-blade installation setup". *J. Phys.: Conf. Ser,* **524**, June, pp. 1–12.

[5] Gaunaa, M., Heinz, J., and Skrzypiński, W., 2016. "Toward an Engineering Model for the Aerodynamic Forces Acting on Wind Turbine Blades in Quasisteady Standstill and Blade Installation Situations". *J. Phys.: Conf. Ser.,* **753**, Sept., pp. 1–12.

[6] Kuijken, L., 2015. "Single Blade Installation for Large Wind Turbines in Extreme Wind Conditions". Master of Science Thesis, TU Delft; DTU.

[7] Wang, Y., Tian, D., and He, W., 2013. "Computation of Hoisting Forces on Wind Turbine Blades Using Computation Fluid Dynamics". *Applied Mechanics and Materials,* **446-447**, Nov., pp. 452–457.

[8] Stewart, G., and Lackner, M., 2013. "Offshore wind turbine load reduction employing optimal passive tuned mass damping systems". *IEEE transactions on control systems technology,* **21**(4), pp. 1090–1104.

[9] Stewart, G. M., and Lackner, M. A., 2014. "The impact of passive tuned mass dampers and wind–wave misalignment on offshore wind turbine loads". *Engineering Structures, 73*, pp. 54–61.

[10] Lackner, M. A., and Rotea, M. A., 2011. "Passive structural control of offshore wind turbines". *Wind Energy, 14*(3), pp. 373–388.

[11] Colwell, S., and Basu, B., 2009. "Tuned liquid column dampers in offshore wind turbines for structural control". *Engineering Structures, 31*(2), pp. 358–368.

[12] Brodersen, M. L., and Hogsberg, J., 2014. "Damping of offshore wind turbine tower vibrations by a stroke amplifying brace". In *Eera Deepwind' 2014, 11th Deep Sea Offshore Wind R&d Conference*, T. Kvamsdal, M. Muskulus, and J. O. Tande, eds., Vol. 53. Elsevier Science Bv, Amsterdam, pp. 258–267. WOS:000345418400026.

[13] Sun, C., Jahangiri, V., and Sun, H., 2019. "Performance of a 3d pendulum tuned mass damper in offshore wind turbines under multiple hazards and system variations". *Smart Structures and Systems, 24*(1), July, pp. 53–65.

[14] Sun, C., and Jahangiri, V., 2019. "Fatigue damage mitigation of offshore wind turbines under real wind and wave conditions". *Engineering Structures, 178*, Jan., pp. 472–483.

[15] Sun, C., and Jahangiri, V., 2018. "Bi-directional vibration control of offshore wind turbines using a 3d pendulum tuned mass damper". *Mechanical Systems and Signal Processing, 105*, May, pp. 338–360.

[16] Jahangiri, V., and Sun, C., 2019. "Integrated bi-directional vibration control and energy harvesting of monopile offshore wind turbines". *Ocean Engineering, 178*, Apr., pp. 260–269.